Neuroanatomical changes observed over the course of a human pregnancy

Laura Pritschet[1*], Caitlin M. Taylor[1], Daniela Cossio[2], Tyler Santander[1], Hannah Grotzinger[1], Joshua Faskowitz[3], Daniel A. Handwerker[3], Evan Layher[1], Elizabeth R. Chrastil[2+*], & Emily G. Jacobs[1,4+*]

[1]Department of Psychological & Brain Sciences, University of California, Santa Barbara, CA

[2]Department of Neurobiology and Behavior, University of California, Irvine, CA

[3]Section on Functional Imaging Methods, Laboratory of Brain and Cognition, National Institute of Mental Health, National Institutes of Health, Bethesda, MD

[4]Neuroscience Research Institute, University of California, Santa Barbara, CA

[+]these authors contributed equally to the work

*laura.pritschet@psych.ucsb.edu, chrastil@uci.edu, emily.jacobs@psych.ucsb.edu

Author Contributions: The overall study was conceived by L.P., C.M.T., E.R.C., and E.G.J.; L.P., C.M.T., D.C., T.S., E.L., E.R.C., and E.G.J. performed the experiments; data analysis strategy was conceived by L.P., C.M.T., D.C., T.S., J.F., D.A.H., E.R.C. and E.G.J., then implemented by L.P., C.M.T., and D.C.; L.P., C.M.T., H.G., D.C., E.R.C, and E.G.J. wrote the manuscript; T.S., J.F., D.A.H., and E.L. edited the manuscript.

Competing Interest Statement: None.

Keywords: pregnancy, brain structure, MRI, sex steroid hormones, precision imaging, women's health

This file includes: Main Text, Figures 1–3

Pregnancy is a period of profound hormonal and physiological change experienced by millions of women annually, yet the neural changes unfolding in the maternal brain throughout gestation have not been studied in humans. Leveraging precision imaging, we mapped neuroanatomical changes in an individual from preconception through two years postpartum. Pronounced decreases in gray matter volume and cortical thickness paired with increases in white matter microstructure were evident across the brain, with few regions untouched by the transition to motherhood.

Each year, ~140 million women around the globe experience one of the most transformative events of their lifetime—pregnancy (WHO, 2022). Over an approximately 40-week gestational window the maternal body undergoes profound physiological adaptations to support the development of the fetus, including increases in plasma volume, metabolic rate, oxygen consumption, and immune regulation (Thornburg et al., 2015). These rapid adaptations are initiated by hundred- to thousand-fold increases in hormone production, including estrogen and progesterone. These neuromodulatory hormones also drive significant reorganization of the central nervous system. New mechanistic insights from animal models converge on pregnancy as a period of remarkable neuroplasticity (Puri et al., 2023; Celik et al., 2022; Barrière et al., 2021; Haim et al., 2017; Brunton & Russell et al., 2008). In humans, reductions in gray matter volume (GMV) have been observed postpartum (Hoekzema et al., 2017, 2022; Martínez-García, et al., 2021a), particularly in regions central to theory-of-mind processing (Hoekzema et al., 2017). These GMV changes persist at six years postpartum (Martínez-García et al., 2021b) and are traceable decades later (De Lange et al., 2019; Orchard et al., 2020, 2023), underscoring the permanence of this major remodeling event. Yet, the changes that occur within the maternal brain during gestation itself are virtually unknown.

Here, we conducted the first precision imaging study of pregnancy in which a healthy 38-year-old primiparous woman underwent 26 MRI scans and venipuncture beginning 3 weeks pre-conception through two years postpartum. We observed widespread reductions in GMV and cortical thickness (CT) occurring in step with the dramatic rise in sex hormone production across gestation. Next, high-resolution imaging and segmentation of the medial temporal lobe suggest specific volumetric reductions within parahippocampal cortex. In contrast to widespread decreases in GMV, correlational tractography analyses revealed non-linear increases in white matter quantitative anisotropy (QA) throughout the brain —indicating greater tract integrity— as gestational week progressed. Together, these findings are the first to reveal the highly dynamic changes that unfold in the human brain across pregnancy, raising the possibility that the adult brain undergoes extensive remodeling well into adulthood.

Serological evaluations captured canonical hormone fluctuations characteristic of the prenatal, perinatal, and postnatal periods (**Fig. 1A–C**). Serum hormone concentrations increased significantly over the course of pregnancy and dropped precipitously postpartum (pre-conception: estradiol (E) = 3.42 pg/mL, progesterone (P) = 0.84 ng/mL; 3 weeks prior to

parturition: E = 12,400 pg/mL, P = 103 ng/mL; 3 months after parturition: E = 11.50 pg/mL, P = 0.04 ng/mL).

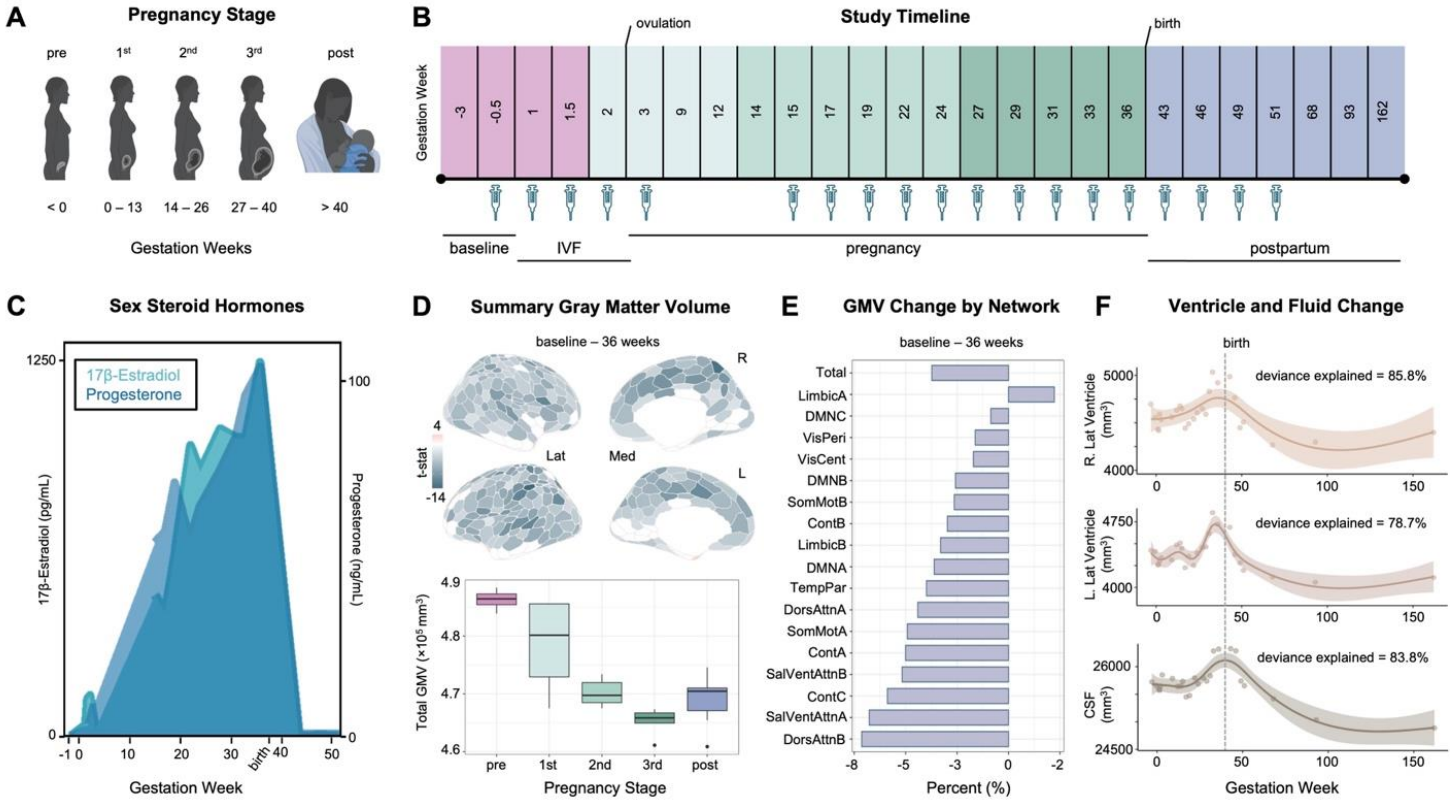

Figure 1. Precision imaging reveals neuroanatomical changes throughout gestation. A) Standard medical demarcations for pregnancy stages (e.g., trimesters) by gestation week. **B)** A healthy 38-year-old primiparous woman underwent 26 scanning sessions from 3 weeks preconception through two years postpartum. Scans were distributed throughout preconception (4 scans), first trimester (4 scans), second trimester (6 scans), third trimester (5 scans), and postpartum (7 scans); colors indicate pregnancy stage. The participant underwent in-vitro fertilization (IVF) to achieve pregnancy, allowing for precise mapping of ovulation, conception, and gestation week. Serological assessments to evaluate steroid hormones were available for 19 sessions (see *Methods*). **C)** Sex steroid hormones increased significantly over the course of pregnancy and dropped precipitously postpartum, as is characteristic of the pre- and postnatal periods. **D)** Multivariate regression analyses reveal largely negative relationships between gestation week and regional GMV (top), with only a minority of regions unaffected or increasing over the gestational window. All associations presented here were corrected for multiple comparisons (FDR at $q < 0.05$). Summarizing GMV across the entire study (baseline – 162 weeks) suggests slight recovery in the postpartum period (bottom). Error bars indicate ± SEM. **E)** Average network change was calculated by estimating GMV change from baseline – 36 weeks gestation. Attention and Control Networks appeared most affected. **F)** Left and right lateral ventricle and cerebrospinal fluid volumes displayed non-linear increases across gestation, with a notable rise in the second and third trimester before dropping sharply postpartum. Shaded regions represent a 95% confidence interval; dashed line indicates parturition. *Abbreviations*: IVF = in-vitro fertilization; Lat = lateral; Med = medial; t-stat = test statistic; GMV = gray matter volume; DMN = Default Mode Networks; VisPeri = Visual Peripheral Network; SomMot = Somatomotor Networks; VisCent = Visual Central Network; Cont = Control Networks; TempPar = Temporal Parietal Network; DorsAttn = Dorsal Attention Networks; SalVentAttn = Salience / Ventral Attention Networks; CSF = cerebrospinal fluid

To begin, we quantified the neuroanatomical changes that unfold during gestation itself (baseline–36 weeks pregnant; 19 scans). Changes in GMV were near-ubiquitous across the cortical mantle (**Fig. 1D**), with strong negative associations between gestational week and total GMV (r = -0.90, p < .001, *95% CI = -0.96,-0.75, total change* = -3.5%). Most large-scale brain networks exhibited decreases in GMV (**Fig. 1E, Table S1**); indeed, 80% of the 400 regions of interest (ROIs) demonstrated negative relationships with GMV throughout gestation (**Fig. 1D**, **Table S2**). Together, these results provide evidence of a global decrease in cortical volume across pregnancy. A handful of sensory and attention subnetworks were particularly sensitive to gestation, such as the Control (B), Salience/Ventral Attention (A), Dorsal Attention (B), Default (A), and Somatomotor (A,B) Networks; each significantly covarying with gestation week even after accounting for total GMV change. Regions driving these network-level changes include the inferior parietal lobe, post central gyri, insulae, prefrontal cortex, posterior cingulate, and somatosensory cortex (**Fig. 2**, **Table S2**). These regions and associated brain networks appear to decrease in volume at a faster rate than the rest of the brain throughout pregnancy. GMV reductions were also significantly correlated with the participant's sex hormone concentrations. (**Table S1**). A highly similar pattern of results was observed when examining pregnancy-related cortical thickness changes (**Fig. S1, Tables S3–4**).

In contrast, GMV within regions of the Default Mode (C), Limbic (A,B), and Visual Peripheral Networks buck the global trend by slightly increasing (e.g., temporal poles), remaining constant (e.g., orbitofrontal cortex), or reducing at a much slower rate (e.g., extrastriate) than total GMV (**Fig. 1E, Tables S1–4**). Cortical thickness changes in these regions exhibit similar patterns (**Tables S3–4**).

Consistent with the broader cortical reductions in GMV, high-resolution medial temporal lobe segmentations revealed decreased parahippocampal cortex (PHC) volume (r = -0.79, FDR-corrected at q < 0.05) across gestation (**Fig. 3B**). Results remained significant after proportional volume correction for total GMV. Notably, there was no significant change in other hippocampal and medial temporal cortical subregions, or in gross hippocampal volume (**Fig. S3**, **Table S6**).

In contrast to decreasing global GMV, correlational tractography of white matter—which tests for linear trends in the data— revealed increasing microstructural integrity (quantitative anisotropy, QA) across the whole brain during gestation, concomitant with the rise in 17ß-estradiol and progesterone (*FDRs* < .001) (**Fig. 3C, Fig. S4**). Tracts displaying robust

correlations with gestational week include the cingulum bundle, middle and superior longitudinal fasciculus, corpus callosum, and arcuate fasciculus (**Fig. 3D**, see **Table S6** for complete list).

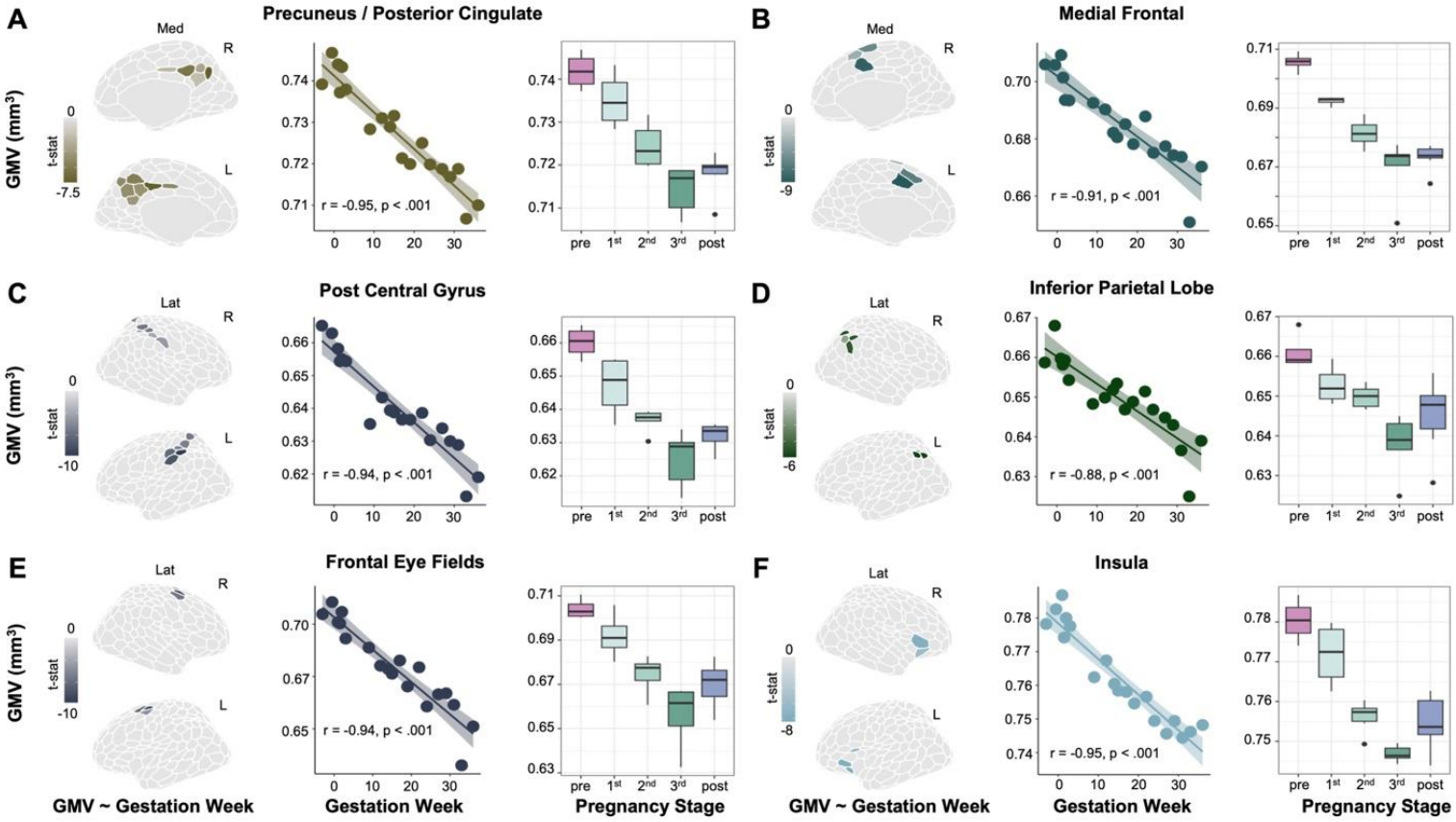

Figure 2. Pronounced GMV changes across gestation. A–F) Six representative regions that decline in volume at a rate greater than the global decrease. For each panel, we display results of a multivariate regression revealing significant associations between clustered ROI GMV and gestation week (left), Pearson's product-moment correlations between the average GMV of the ROIs and gestation week (middle), and summary ROI GMV by pregnancy stage across the whole study (right). All statistical tests were corrected for multiple comparisons (FDR at $q < 0.05$). Error bars indicate ± SEM. ROI subregions are color-coded by network affiliation (see **Fig. S2**). N.b., shown here are raw data values (see **Table S3** and **Supplementary File 2** for exhaustive list).

Next, we widened the aperture to capture changes extending into the postpartum period (baseline–2 years postpartum; 26 scans), revealing non-linear patterns for several brain measures. Global QA for white matter increased throughout the first and second trimester before returning to baseline levels in the postpartum period (*whole brain QA*, $F = 6.791$, $p < .002$, *deviance explained* = 71.9%) (**Fig. 3E**). Similarly, we observed non-linear patterns of lateral ventricle expansion *(left*, $F = 7.70$, $p < .001$, *deviance explained* = 78.7%; *right*, $F = 11.99$, $p <$

.001, *deviance explained* = 85.8%) and increased cerebrospinal fluid (CSF; $F = 13.32$, $p < .001$, *deviance explained* = 83.8%), rising in the second and third trimester before dropping sharply in postpartum (**Fig. 1F**). After linearly decreasing during gestation, GMV and CT appear to partially rebound postpartum.

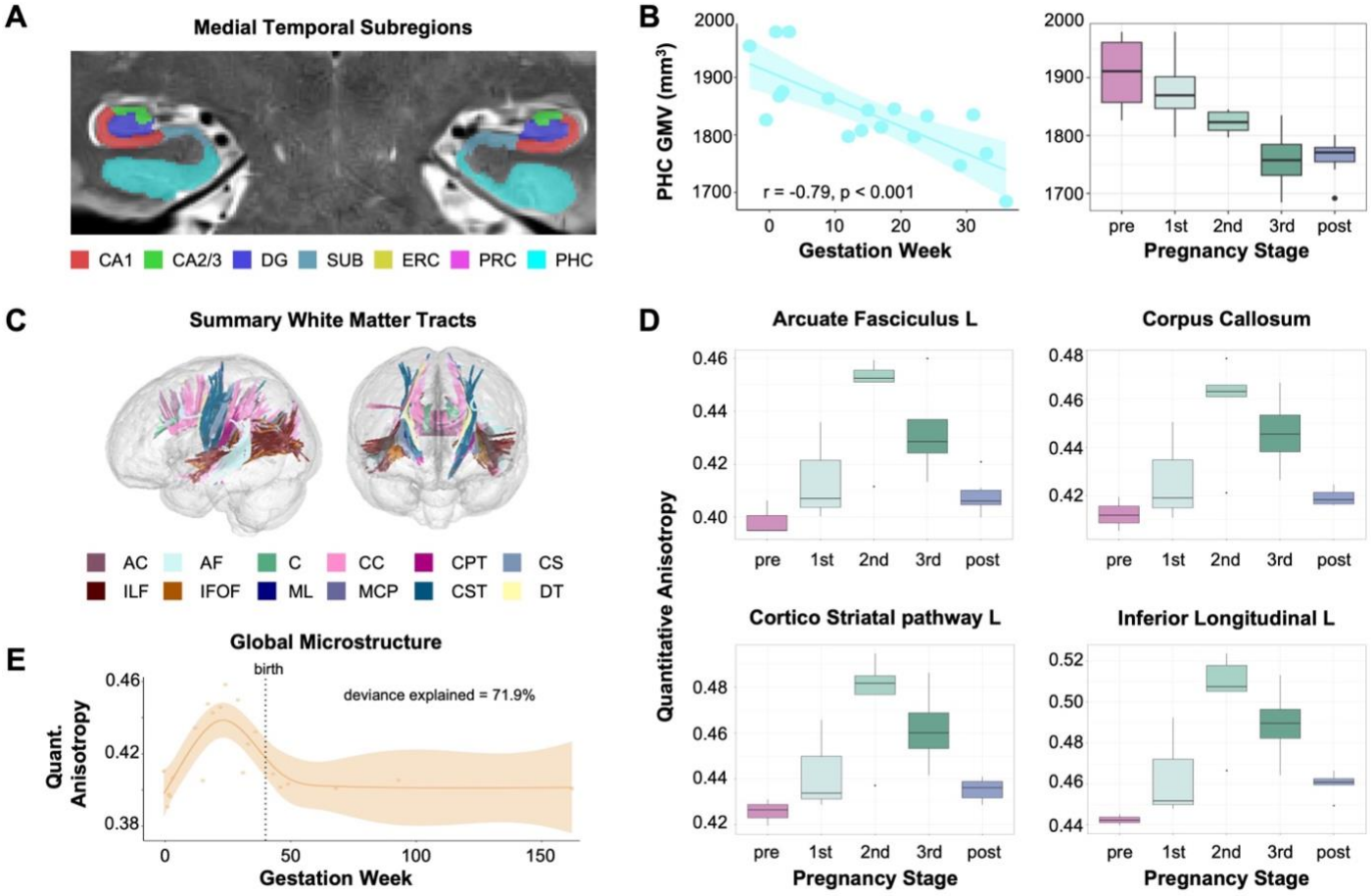

Figure 3. Hippocampal subfields and white matter microstructure across gestation. A) Sample image of medial temporal lobe segmentation determined via manual editing of the output of the Automatic Segmentation of Hippocampal Subfields (ASHS) software package. The participant's hippocampus and surrounding cortex were segmented into seven bilateral subregions. **B)** Parahippocampal cortex (PHC) volume was negatively associated with gestation week (left) and did not return to baseline postpartum (right). Error bars indicate ± SEM. **C)** White matter tracts demonstrate increasing quantitative anisotropy in relation to gestation week as determined by correlational tractography analysis. **D)** Summary of quantitative anisotropy (QA) values by pregnancy stage for representative ROIs identified as significantly associated with gestation week. Tractometry was used to extract quantitative anisotropy values. Error bars indicate ± SEM. **E)** Whole brain QA displayed non-linear patterns of growth across gestation. Shaded region represents the 95% confidence interval. Abbreviations: AC= Anterior Commissure; PHC = parahippocampal cortex; GMV = gray matter volume; AF = arcuate fasciculus; CC = corpus callosum; ILF = inferior longitudinal fasciculus; CS = corticostriatal tracts; CST = corticospinal tracts; CPT = Corticopontine tracts; IFOF = inferior frontal occipital fasciculus; ML = medial lemniscus; MCP = middle cerebellar peduncle; DT = dentothalamic tract; QA = quantitative anisotropy

Emerging findings across taxa establish pregnancy as a remarkable period of synaptic plasticity, underscoring the brain's ability to undergo neuroanatomical changes beyond adolescence (Dulac et al., 2014; Carmona et al., 2019; Hoekzema et al., 2017, 2022; Martínez-García, et al., 2021a; Pawluski et al., 2022). Investigations that compare women pre- and postpartum provide the strongest evidence to date that the human brain undergoes such neural changes (Martínez-García 2021b, Orchard et al., 2023), and our results are largely consistent with the findings from those designs. But what about pregnancy itself? Over what time-course do anatomical changes in the maternal brain manifest? Are they tied to the substantial increase in sex hormone production? Here, we begin to address these outstanding questions. This paper and corresponding open-access dataset offer neuroscientists the first atlas of the human brain across gestation.

Our findings suggest that the gestational period is characterized by sweeping decreases in gray matter volume, cortical thinning, and enhanced white matter microstructural integrity that unfold week by week. Some of these changes persist at two years postpartum (e.g., global reductions in GMV, CT), while others, including markers of white matter integrity, appear to be transient. Ventricle expansion and contraction parallel these cortical changes. These patterns, paired with increased CSF volume, could reflect increased water retention and subsequent compression of cortical tissue. However, regional variation in GMV, CT, and QA changes hint at cellular underpinnings, such as alterations in glia or neuron number, synaptic density, and myelination. Future studies of the relationship between fluid dynamics and volumetric changes will help clarify the factors that drive global neural changes during pregnancy; such insights have broad implications for maternal health (e.g., neurological effects tied to pre-eclampsia or edema).

Dynamic neural changes occurred *within* the pregnancy window itself, a nuance not captured by studies limited to pre- versus post-pregnancy comparisons. For example, we observed large increases in white matter microstructural integrity (QA) throughout the first and second trimester of pregnancy, but these measures fully returned to baseline values by the first postpartum scan. This pattern may explain why previous studies report no pregnancy-related differences in white matter tractography (Hoekzema, 2022). Other measures, such as GMV and CT, decreased throughout gestation and displayed only a modest rebound postpartum. Together, these non-linear patterns suggest that only quantifying pre- and postpartum brain structure may overlook the full dynamic range of changes that unfold within the gestational window — and

underrepresent the brain's metamorphosis during pregnancy. Further, although global brain changes were the norm, some regions displayed notable stability (e.g., the majority of medial temporal lobe and extrastriate cortex), which merits further study. Similar precision imaging studies have captured dynamic brain reorganization across other neuroendocrine transitions, such as the menstrual cycle (see review: Pritschet et al., 2021), underscoring the powerful role sex steroid hormones play in shaping the mammalian brain (Taxier et al., 2020). Endocrine changes across pregnancy dwarf those that occur across the menstrual cycle, which highlights the critical need to map the brain's response to this unique hormonal milieu.

The neuroanatomical changes that unfold during matrescence have broad implications for understanding individual differences in parental behavior (Dulac et al., 2014; Hoekzema et al., 2017; Kohl et al., 2018), vulnerability to mental health disorders (Pawluski et al., 2017; Barba-Müller et al., 2019) and patterns of brain aging (de Lange et al., 2019; Barth & de Lange, 2020; Orchard et al., 2020, 2023). Decreases in GMV may reflect "fine-tuning" of the brain by neuromodulatory hormones in preparation for parenthood (Pawluski et al., 2022). For example, GMV reduction is pronounced in areas of the brain important for social cognition and the magnitude of these changes correspond with increased parental attachment behaviors (Hoekzema et al., 2017). Similarly, we observed the greatest GMV change in regions within attention, sensory, and default mode networks (see also: Paternina-Die et al., 2023). Quantifying the rate of change within these circuits could be key for understanding the behavioral adaptions that emerge during and after pregnancy, such as honing the brain's visual and auditory responses to infant cues and elicitation of maternal behavior.

This precision imaging study mapped neuroanatomical changes across pregnancy in a single individual. These findings provide critical rationale for conducting further dense-sampling studies of demographically enriched cohorts to determine the universality and idiosyncrasy of these adaptations and their role in maternal health. For example, this approach could determine whether the pace of pregnancy-induced neuroanatomical changes drives divergent brain health outcomes in women, as may be the case during other rapid periods of brain development (Tooley et al. 2021). One in five women experiences postpartum depression (Wang et al., 2021), and while the first FDA-approved treatment is now available (Deligiannidis et al., 2023), early detection remains elusive. Precision imaging studies could offer clues about an individual's risk for or resilience to postpartum depression prior to symptom onset. Neuroscientists and clinicians

also lack tools to facilitate detection and treatment of neurological disorders that co-occur, worsen, or remit with pregnancy, such as epilepsy, headaches, multiple sclerosis, and intracranial hypertension (Shehata et al., 2004). This new area of study—precision mapping of the maternal brain—lays the groundwork for a greater understanding of the subtle and sweeping structural, functional, behavioral, and clinical changes that unfold across gestation. Such pursuits will advance our basic understanding of the human brain and its remarkable ability to undergo protracted plasticity in adulthood.

References

1. Barba-Müller, E., Craddock, S., Carmona, S., & Hoekzema, E. (2019). Brain plasticity in pregnancy and the postpartum period: links to maternal caregiving and mental health. *Archives of women's mental health*, *22*, 289-299.

2. Barrière, D. A., Ella, A., Szeremeta, F., Adriaensen, H., Même, W., Chaillou, E., Migaud, M., Même, S., Lévy, F., & Keller, M. (2021). Brain orchestration of pregnancy and maternal behavior in mice: A longitudinal morphometric study. *NeuroImage*, *230*, 117776.

3. Barth, C., & de Lange, A.-M. G. (2020). Towards an understanding of women's brain aging: The immunology of pregnancy and menopause. *Frontiers in Neuroendocrinology*, *58*, 100850.

4. Been, L. E., Sheppard, P. A., Galea, L. A., & Glasper, E. R. (2022). Hormones and neuroplasticity: A lifetime of adaptive responses. *Neuroscience & Biobehavioral Reviews*, *132*, 679-690

5. Brunton, P. J., & Russell, J. A. (2008). The expectant brain: Adapting for motherhood. *Nature Reviews Neuroscience*, *9*(1), 11–25.

6. Carmona, S., Martínez-García, M., Paternina-Die, M., Barba-Müller, E., Wierenga, L. M., Alemán Gómez, Y., Pretus, C., Marcos-Vidal, L., Beumala, L., Cortizo, R., Pozzobon, C., Picado, M., Lucco, F., García-García, D., Soliva, J. C., Tobeña, A., Peper, J. S., Crone, E. A., Ballesteros, A., … Hoekzema, E. (2019). Pregnancy and adolescence entail similar neuroanatomical adaptations: A comparative analysis of cerebral morphometric changes. *Human Brain Mapping*, *40*(7), 2143–2152.

7. Celik, A., Somer, M., Kukreja, B., Wu, T., & Kalish, B. T. (2022). The Genomic Architecture of Pregnancy-Associated Plasticity in the Maternal Mouse Hippocampus. *Eneuro*, *9*(5).

8. de Lange, A.-M. G., Kaufmann, T., van der Meer, D., Maglanoc, L. A., Alnæs, D., Moberget, T., Douaud, G., Andreassen, O. A., & Westlye, L. T. (2019). Population-based neuroimaging reveals traces of childbirth in the maternal brain. *Proceedings of the National Academy of Sciences*, *116*(44), 22341–22346.

9. Deligiannidis, K. M., Meltzer-Brody, S., Maximos, B., Peeper, E. Q., Freeman, M., Lasser, R., ... & Doherty, J. (2023). Zuranolone for the Treatment of Postpartum Depression. *American Journal of Psychiatry*, appi-ajp.

10. Dulac, C., O'Connell, L. A., & Wu, Z. (2014). Neural control of maternal and paternal behaviors. *Science*, *345*(6198), 765–770.

11. Haim, A., Julian, D., Albin-Brooks, C., Brothers, H. M., Lenz, K. M., & Leuner, B. (2017). A survey of neuroimmune changes in pregnant and postpartum female rats. Brain, behavior, and immunity, 59, 67-78.

12. Hoekzema, E., Barba-Müller, E., Pozzobon, C., Picado, M., Lucco, F., García-García, D., Soliva, J. C., Tobeña, A., Desco, M., Crone, E. A., Ballesteros, A., Carmona, S., & Vilarroya, O. (2017). Pregnancy leads to long-lasting changes in human brain structure. *Nature Neuroscience*, *20*(2), 287–296.

13. Hoekzema, E., van Steenbergen, H., Straathof, M., Beekmans, A., Freund, I. M., Pouwels, P. J. W., & Crone, E. A. (2022). Mapping the effects of pregnancy on resting state brain activity, white matter microstructure, neural metabolite concentrations and grey matter architecture. *Nature Communications*, *13*(1), 6931.

14. Kohl, J., Babayan, B. M., Rubinstein, N. D., Autry, A. E., Marin-Rodriguez, B., Kapoor, V., Miyamishi, K., Zweifel, L. S., Luo, L., Uchida, N., & Dulac, C. (2018). Functional circuit architecture underlying parental behaviour. *Nature*, *556*(7701), Article 7701.

15. Martínez-García, M., Paternina-Die, M., Desco, M., Vilarroya, O., & Carmona, S. (2021a). Characterizing the Brain Structural Adaptations Across the Motherhood Transition. *Frontiers in Global Women's Health*, *2*(742775).

16. Martínez-García, M., Paternina-Die, M., Barba-Müller, E., Martín de Blas, D., Beumala, L., Cortizo, R., Pozzobon, C., Marcos-Vidal, L., Fernández-Pena, A., & Picado, M. (2021b). Do Pregnancy-Induced Brain Changes Reverse? The Brain of a Mother Six Years after Parturition. *Brain Sciences*, *11*(2), 168.

17. Orchard, E. R., Ward, P. G. D., Chopra, S., Storey, E., Egan, G. F., & Jamadar, S. D. (2020). Neuroprotective Effects of Motherhood on Brain Function in Late Life: A Resting-State

fMRI Study. *Cerebral Cortex*, 1270-1283.

18. Orchard, E. R., Rutherford, H. J. V., Holmes, A. J., & Jamadar, S. D. (2023). Matrescence: Lifetime impact of motherhood on cognition and the brain. *Trends in Cognitive Sciences*.

19. Paternina-Die, M., Martínez-García, M., de Blas, D. M., Noguero, I., Servin-Servet, C., Pretus, C., ... & Carmona, S. (2023). Women's neuroplasticity during gestation, childbirth, and postpartum (preprint). https://doi.org/10.21203/rs.3.rs-2723150/v1

20. Pawluski, Jodi L., Joseph S. Lonstein, and Alison S. Fleming. "The neurobiology of postpartum anxiety and depression." Trends in Neurosciences 40.2 (2017): 106-120.

21. Pawluski, J. L., Hoekzema, E., Leuner, B., & Lonstein, J. S. (2021). Less Can Be More: Fine Tuning the Maternal Brain. *Neuroscience & Biobehavioral Reviews*.

22. Pritschet, L., Taylor, C. M., Santander, T., & Jacobs, E. G. (2021). Applying dense-sampling methods to reveal dynamic endocrine modulation of the nervous system. *Current opinion in behavioral sciences*, *40*, 72-78.

23. Puri, T. A., Richard, J. E., & Galea, L. A. M. (2023). Beyond sex differences: Short- and long-term effects of pregnancy on the brain. *Trends in Neurosciences*.

24. Shehata, H. A., & Okosun, H. (2004). Neurological disorders in pregnancy. *Current Opinion in Obstetrics and Gynecology*, *16*(2), 117-122.

25. Taxier, L. R., Gross, K. S., & Frick, K. M. (2020). Oestradiol as a neuromodulator of learning and memory. *Nature Reviews Neuroscience*, *21*(10), 535-550.

26. Thornburg, K. L., Bagby, S. P., & Giraud, G. D. (2015). Maternal Adaptations to Pregnancy. In *Knobil and Neill's Physiology of Reproduction* (pp. 1927–1955). Elsevier, Inc.

27. Tooley, U.A., Bassett, D.S., & Mackey, A.P. (2021). Environmental influences on the pace of brain development. Nature Reviews Neuroscience, 22, 372-384.

28. Wang, Z., Liu, J., Shuai, H., Cai, Z., Fu, X., Liu, Y., ... & Yang, B. X. (2021). Mapping global prevalence of depression among postpartum women. *Translational psychiatry*, *11*(1), 543.

29. World Health Organization (2022). "*Maternal, newborn, child and adolescent health and ageing"*

Materials and Methods (Online only)

Participant

Our participant (author E.R.C.) was a healthy 38-year-old primiparous woman who underwent in-vitro fertilization (IVF) to achieve pregnancy. Previous studies reported no observable differences in neural changes pre- to post-pregnancy between women who conceived naturally versus women who conceived via IVF (Hoekzema et al., 2017), and doing so provides a controlled way of monitoring pregnancy status. The participant nursed through one-year postpartum, and had no history of neuropsychiatric diagnosis, endocrine disorders, prior head trauma or history of smoking. The participant gave written informed consent and the study was approved by the University of California, Irvine Human Subjects Committee.

Study Design

The participant underwent 26 magnetic resonance imaging (MRI) scanning sessions from 3 weeks prior to conception through two years postpartum (162 weeks), during which high-resolution anatomical and diffusion spectrum imaging scans of the brain were acquired. Scans were distributed throughout this period, including pre-pregnancy (4 scans), first trimester (4 scans), second trimester (6 scans), third trimester (5 scans), and postpartum (7 scans) (**Fig. 1B**). The first 6 sessions took place at the UCSB Brain Imaging Center (BIC), the final 20 sessions took place at the UCI Facility for Imaging and Brain Research (FIBRE). The MRI protocol, scanner (Siemens 3T Prisma), and software (version MR E11) were identical across sites. To ensure the robustness of the findings, after the final study session the subject completed two additional back-to-back validation scans at UCSB and UCI within a 12-hour window to assess reliability between scanners. Intraclass correlation coefficients (two-way, random effects, absolute agreement, single rater) reveal 'excellent' test-retest reliability between scanners, including: ROI-level GMV (*ICC* = 0.97, *95% CI*: 0.80–0.99); ROI-level CT (*ICC* = 0.96, *95% CI*: 0.90–0.98); MTL subfield volume (*ICC* = 0.99, *95% CI:* 0.97–0.99); and ROI-level QA (*ICC* = 0.94, *95% CI:* 0.91–0.97). Further, when examining the relationship between gestation week, cortical and subcortical GMV among UCI-only gestational sessions, consistent findings were observed (**Fig. S5**), indicating that site differences are highly unlikely to have contributed meaningfully to the observed effects.

Endocrine Procedures

The participant underwent a blood draw (n = 19, **Fig. 1B**) prior to MRI scanning. Sex steroid concentrations were determined via ultra-sensitive liquid chromatography–mass spectrometry (LC-MS) at the Brigham and Women's Hospital Research Assay Core (BRAC). Assay sensitivities, dynamic range, and intra-assay coefficients of variation were as follows: estradiol: 1.0 pg/ml, 1–500 pg/ml, <5% relative standard deviation (RSD); progesterone: 0.05 ng/ml, 0.05–10 ng/ml, 9.33% RSD. Serological samples were not acquired in five sessions due to scheduling conflicts with UC Irvine's Center for Clinical Research.

MRI Acquisition

Magnetic resonance imaging (MRI) scanning sessions at the University of California, Santa Barbara and Irvine were conducted on 3T Prisma scanners equipped with 64-channel phased-array head/neck coil (of which 50 coils are used for axial brain imaging). High-resolution anatomical scans were acquired using a T1-weighted (T1w) magnetization prepared rapid gradient echo (MPRAGE) sequence (TR = 2500 ms, TE = 2.31 ms, T1 = 934 ms, flip angle = 7°, 0.8 mm thickness) followed by a gradient echo fieldmap (TR = 758 ms; TE1 = 4.92 ms; TE2 = 7.38 ms; flip angle = 60°). A T2-weighted (T2w) turbo spin echo (TSE) scan was also acquired with an oblique coronal orientation positioned orthogonally to the main axis of the hippocampus (TR/TE = 9860/50 ms, flip angle = 122°, 0.4 × 0.4 mm^2 in-plane resolution, 2 mm slice thickness, 38 interleaved slices with no gap, total acquisition time = 5:42 min). The DSI protocol sampled the entire brain with the following parameters: single phase, TR = 4300 ms, echo time = 100.2 ms, 139 directions, b-max = 4990, FoV = 259 x 259 mm, 78 slices, 1.7986 x 1.7986 x 1.8 mm voxel resolution. These images were linearly registered to the whole-brain T1w MPRAGE image. A custom foam headcase was used to provide extra padding around the head and neck, as well as to minimize head motion. A custom-built sound-absorbing foam girdle was placed around the participant's waist to attenuate sound near the fetus during second and third trimester scanning.

Image Processing

Cortical Volume and Thickness

Cortical thickness and gray matter volume were measured with Advanced Normalization Tools version 2.1.0 (ANTs) (Avants et al., 2011). We first built a custom subject-specific template (SST) (*antsMultivariateTemplateConstruction2*) and tissue priors (*antsCookTemplatePriors*) based on our subject's two pre-conception whole-brain T1-weighted scans to examine neuroanatomical changes relative to the subject's pre-pregnancy baseline. We used labels from the OASIS population template, provided by ANTs, as priors for this step. For each session, the structural image was processed and registered to the SST using the ANTs cortical thickness pipeline (*antsCorticalThickness*). This begins with an N4 bias field correction for field inhomogeneity, then brain extraction using a hybrid registration/segmentation method (see Tustison et al., 2014). Tissue segmentation was performed using Atropos (Avants et al., 2011) to create tissue masks of cerebrospinal fluid (CSF), gray matter, white matter, and deep gray matter. Atropos allows prior knowledge to guide the segmentation algorithm, and we used labels from our SST as priors to minimize warping and remain in native subject space. Cortical thickness measurements were then estimated using the DiReCT algorithm (Das et al., 2009), which estimates the gray/white matter interface and the gray matter/CSF interface and computes a diffeomorphic mapping between the two interactions, from which thickness is derived. Each gray matter tissue mask was normalized to the template and multiplied to a Jacobian image that was computed via affine and non-linear transforms. Summary, regional-level estimates of CT, GMV, and CSF for each scan were obtained by taking the first eigenvariate (akin to a 'weighted mean', Friston et al., 2006) across all voxels within each parcel of the Schaefer 400-region atlas (Schaefer et al., 2018). We then averaged ROIs across networks, which were defined by the 17-network Schaefer scheme (Yeo et al., 2011; Schaefer et al., 2018). Global measures of CT, GMV, and CSF were computed for each session by summing across all voxels within the respective output image. Our findings held when using an SST derived from all 26 MRIs (pre- through postpartum), as well as when estimating the mean (vs. weighted mean) of all voxels within each parcel. The ANTs CT pipeline is highly validated with good test-retest reproducibility and improved ability to predict variables such as age and gender from region-wise CT measurements compared to surface-based FreeSurfer (Tustison et al., 2014). However, to reproduce our findings across software packages, we also ran the T1w data through the

longitudinal FreeSurfer cortical thickness pipeline (Dale et al., 1999), which corroborated our findings using both the Schaefer 400-cortical atlas (**Tables S1** and **S3**) and the popular Desikan-Killiany cortical atlas (Desikan et al., 2004, see **Fig S5**); lateral ventricle volume estimates were derived from this output. A complete reporting of findings can be found in **Supplementary File 2**.

Mean framewise displacement (FWD) estimates from gestation sessions with a 10-minute resting state scan (n = 17) were used to indirectly assess whether motion increased throughout pregnancy. Average FWD (millimeters) was extremely minimal across the entire experiment (*M* = 0.13, *SD* = 0.02, *range* = 0.09–0.17) and varied only slightly by pregnancy stage (pre: *M* = 0.11, *SD* = 0.004; first: *M* = 0.11, *SD* = 0.01; second: *M* = 0.14, *SD* = 0.02; third: *M* = 0.16, *SD* = 0.007; post: *M* = 0.13, *SD* = 0.01). While mean FWD did correspond with gestation week (r = 0.90, $p < .001$), controlling for this did not alter our main findings (e.g., total GMV and gestation, partial correlation: r = -0.64, p = 0.004) owing to the fact that motion differences between stages were minuscule (**Fig. S6A**).

As a further test of the robustness of the dataset, we ran quality control (QC) assessments on all T1w images using the IQMs pipeline from *MRIQC* (Esteban et al., 2017). Assessments of interest included 1) coefficient of joint variation (CJV), 2) signal-to-noise ratio for gray matter (SNR), and 3) contrast-to-noise ratios (CNR). All QC metrics fell within expected standard ranges (**Fig. S6B–D**). Although correlations existed between gestation week and QC measures (CJV, r = 0.70, $p < .001$; SNR and CNR, r = -0.83, $p < .001$), including these variables in the regression models did not alter our main findings. Gestation remained tied to decreases in GMV, especially within regions belonging to attention and somatosensory networks. When looking across all *MRIQC* outputs, discrepancies were noted in session seven (gestation week nine, first trimester). Removing this day from the analyses only strengthened observed relationships between cortical volume and gestation; however for completeness, data from this day is included in the main findings.

Hippocampal Segmentation

T1- and T2-weighted images (n = 25) were submitted to the automatic segmentation of hippocampal subfields package (ASHS) (Yushkevich et al., 2015) for bilateral parcellation of seven MTL subregions: CA1, CA2/3, dentate gyrus (DG), subiculum (SUB), perirhinal cortex

(PRC), entorhinal cortex (ERC), and parahippocampal cortex (PHC). The ASHS segmentation pipeline automatically segmented the hippocampus in the T2w MRI scans using a segmented population atlas, the Princeton Young Adult 3T ASHS Atlas template (n = 24, mean age 22.5 years; Aly and Turk-Browne, 2016). A rigid-body transformation aligned each T2w image to the respective T1w scan for each day. Using ANTs deformable registration, the T1w was registered to the population atlas. The resulting deformation fields were used to resample the data into the space of the left and right template MTL regions of interest (ROI). Within each template ROI, each of the T2w scans of the atlas package was registered to that day's T2w scan. The manual atlas segmentations were then mapped into the space of the T2w scan, with segmentation of the T2w scan computed using joint label fusion (Wang et al., 2012). Finally, the corrective learning classifiers contained in ASHS were applied to the consensus segmentation produced by joint label fusion. The output of this step is a corrected segmentation of the T2w scan. Further description of the ASHS protocol can be found in (Yushkevich et al., 2015). T2w scans and segmentations were first visually examined using ITK-SNAP (Yushkevich et al., 2006) for quality assurance and then subjected to manual editing in native space using ITK-SNAP (v.3.8.0-b; author CMT). One bilateral segmentation (Scan 15, third trimester) was discarded due to erroneous scan orientation. The anterior extent of the segmented labels was anchored 4 mm (2 slices) anterior to the appearance of the limen insulae, and the posterior extent was anchored to the disappearance of hippocampal gray matter from the trigone of the lateral ventricle. Boundaries between perirhinal, entorhinal, and parahippocampal cortices were established in keeping with the Olsen-Amaral-Palombo (OAP) segmentation protocol (Palombo et al., 2013). In instances where automatic segmentation did not clearly correspond to the underlying neuroanatomy, such as when a certain label was missing several gray matter voxels, manual retouching allowed for individual voxels to be added or removed. All results are reported using the manually retouched subregion volumes to ensure the most faithful representation of the underlying neuroanatomy. Scans were randomized and segmentation was performed in a random order, blind to pregnancy stage. To assess intra-rater reliability for the present analyses, two days underwent manual editing a second time. The generalized Dice similarity coefficient (Crum et al., 2006) across subregions was 0.87 and the Intraclass Correlation Coefficient was 0.97, suggesting robust reliability in segmentation.

White Matter Microstructure

Diffusion scans were preprocessed using the automation software QSIprep version 0.15.3 (Cieslak et al., 2022) and run primarily with the default parameters, with the exceptions '–output resolution 1.8', '–dwi denoise window 5',–force-spatial-normalization', '–hmc model 3dSHORE', '–hmc-transform Rigid', and '–shoreline iters 2'. Twenty-one sessions were preprocessed and analyzed, with the remaining five scans excluded due to missing data or the corresponding field map for distortion correction. T1-weighted (T1w) images were corrected for intensity non-uniformity (*N4BiasFieldCorrection*) and skull-stripped (*antsBrainExtraction*). The images underwent spatial normalization and registration to the ICBM 152 Nonlinear Asymmetrical Template. Finally, brain tissue segmentation of CSF, GM, and WM was performed on each brain-extracted T1w using FMRIB's Automated Segmentation Tool (FAST). Preprocessing of diffusion images began by implementing MP-PCA denoising with a 5-voxel window using MRtrix3's *dwidenoise* function. B1 field inhomogeneity was corrected using *dwibiascorrect* from MRtrix3 with the N4 algorithm. Motion was corrected using the *SHORELine* method. Susceptibility distortion correction was based on GRE field maps. Preprocessed Nifti scans were prepared for tractography using DSI Studio version Chen-2022-07-31 (Yeh et al., 2016). Diffusion images were converted to Source Code files using the DSI studio command line *'--action=src'* and a custom script to convert all images. The diffusion data were reconstructed in MNI space using q-space diffeomorphic reconstruction (Yeh et al., 2011) with a diffusion sampling of 1.25 and output resolution of 1.8mm isotropic. The following output metrics were specified to be included in the output FIB file: quantitative anisotropy (QA) and mean diffusivity (MD). The quality and integrity of reconstructed images were assessed using *`QC1: SRC Files Quality Control`*. First, consistency of image dimension, resolution, DWI count, shell count was checked for each image. Second, each image was assessed for the "neighboring DWI Correlation" which calculates the correlation coefficient of low-b DWI volumes that have similar gradient direction. Lower correlation values may indicate issues with the diffusion signal due to artifacts or head motion. Finally, DSI studio performed an outlier check, labelling images as a "low quality outlier" if the correlation coefficient was greater than 3 standard deviations from the absolute mean. None of our scans were flagged as outliers. The reconstructed subject files were aggregated into one connectometry database per metric.

Statistical Analysis

All statistical analyses were conducted in R (version 3.4.4). To isolate how brain structure changes during pregnancy, the following analyses included sessions from baseline through 36 weeks gestation unless otherwise stated.

Gray Matter Volume & Cortical Thickness

We first computed Pearson's product-moment correlation matrices between the following variables (n = 19 pregnancy scans): gestation week, estradiol, progesterone, total GMV, and the 17 network-level average GMV values. We then ran a multivariate regression analysis predicting ROI-level GMV changes by gestation week. To *identify* which regions were changing at a rate different from the global decrease, we then re-ran the analyses to include total GMV in the regression model. This was extended at the network level, where we ran partial correlations accounting for total GMV. These analyses were then run for cortical thickness. Percent change at the network level was computed by subtracting the final pregnancy value (36 weeks pregnant) from the first pre-pregnancy baseline, then dividing that difference by said first pre-pregnancy baseline value. All analyses underwent multiple comparisons testing (FDR-corrected at $q < 0.05$). Ventricle volume and CSF displayed non-linear patterns across the experiment; therefore, we used generalized additive models (GAM; cubic spline basis), a method of non-parametric regression analysis (R package: *mgcv*), to explore the relationship between ventricles, CSF, and gestation week. For each variable, the GAM model outperformed a linear model fit, as determined by a Chi-squared test. To note, for this analysis, we included all 26 sessions to capture the sharp decline of these measures into postpartum.

Hippocampal Segmentation

To evaluate a linear relationship between time and medial temporal lobe (MTL) subregion volume change, we conducted Pearson's product-moment correlations between gestation week and individual bilateral MTL subregion volumes (average of left and right, n = 7 subfields; N = 17 MTL scans). We had no strong a priori hypothesis that structure–hormone relationships would differ by hemisphere; thus, volumes are reported averaged across hemispheres. As a control, we also computed relative MTL subregion volumes expressed as a percentage of total intracranial volume (sum of whole brain gray, white, and cerebrospinal fluid volumes) calculated

by ASHS. This allowed us to correct for the changes in total intracranial volume, which was linearly correlated with gestation week (r = -.723, p < .0001). Relationships were considered significant only if they met FDR correction with q < 0.05. Finally, we conducted a linear regression to evaluate the relationship between endogenous sex hormones (estrogen and progesterone) and volumes of regions that changed significantly across pregnancy.

Diffusion - White Matter Microstructure

DSI Studio's correlational tractography (Yeh et al., 2016) was used to analyze the relationship between white matter structure and gestational week (n = 15). A truncated model was run to examine the relationship between white matter and sex steroid hormones (n = 10) for the subset of diffusion scans with paired endocrine data. A non-parametric Spearman correlation was used to derive the correlation between gestational week and endocrine factors and our metrics of interest (QA and MD; see **Tables S7–8** and **Fig. S4** for MD results) because the data were not normally distributed. Statistical inference was reached using connectometry, a permutation-based approach that tests the strength of coherent associations found between the local connectome and our variables of interest. It provides higher reliability and replicability by correcting for multiple comparisons. This technique provides a high-resolution characterization of local axonal orientation. The correlational tractography was run with the following parameters: T-score threshold of 2.5, 4 pruning iterations, and a length threshold of 25 voxel distance. To estimate the false discovery rate (FDR), a total of 4000 randomized permutations were applied to obtain the null distribution of the track length. Reported regions were selected based on FDR cutoff (FDR < 0.2, suggested by DSI Studio), and contained at least 10 tracts. For visualization of global QA at each gestational stage, QA values were extracted using DSI Studio's whole brain fiber tracking algorithm and tractometry (Yeh et al., 2016). Finally, we used generalized additive models (cubic spline basis) to explore the non-linearity of QA from pre- through postpartum (N = 21 scans; see GMV analysis).

References

1. Aly, M., & Turk-Browne, N. B. (2016). Attention stabilizes representations in the human hippocampus. *Cerebral Cortex*, *26*(2), 783-796.

2. Avants, B. B., Tustison, N. J., Song, G., Cook, P. A., Klein, A., & Gee, J. C. (2011). A reproducible evaluation of ANTs similarity metric performance in brain image registration. Neuroimage, 54(3), 2033-2044.

3. Cieslak, M., Cook, P. A., He, X., Yeh, F. C., Dhollander, T., Adebimpe, A., ... & Satterthwaite, T. D. (2021). QSIPrep: an integrative platform for preprocessing and reconstructing diffusion MRI data. *Nature methods*, *18*(7), 775-778.

4. Crum, W. R., Camara, O., & Hill, D. L. (2006). Generalized overlap measures for evaluation and validation in medical image analysis. *IEEE transactions on medical imaging*, *25*(11), 1451-1461.

5. Dale, A. M., Fischl, B., & Sereno, M. I. (1999). Cortical surface-based analysis: I. Segmentation and surface reconstruction. Neuroimage, 9(2), 179-194.

6. Das, S. R., Avants, B. B., Grossman, M., & Gee, J. C. (2009). Registration based cortical thickness measurement. Neuroimage, 45(3), 867-879.

7. Desikan, R. S., Ségonne, F., Fischl, B., Quinn, B. T., Dickerson, B. C., Blacker, D., ... & Killiany, R. J. (2006). An automated labeling system for subdividing the human cerebral cortex on MRI scans into gyral based regions of interest. Neuroimage, 31(3), 968-980.

8. Esteban, O., Birman, D., Schaer, M., Koyejo, O. O., Poldrack, R. A., & Gorgolewski, K. J. (2017). MRIQC: Advancing the automatic prediction of image quality in MRI from unseen sites. PloS one, 12(9), e0184661.

9. Friston, K. J., Rotshtein, P., Geng, J. J., Sterzer, P., & Henson, R. N. (2006). A critique of functional localisers. Neuroimage, 30(4), 1077-1087.

10. Palombo, D. J., Amaral, R. S., Olsen, R. K., Müller, D. J., Todd, R. M., Anderson, A. K., & Levine, B. (2013). KIBRA polymorphism is associated with individual differences in hippocampal subregions: evidence from anatomical segmentation using high-resolution MRI. *Journal of Neuroscience*, *33*(32), 13088-13093.

11. Schaefer, A., Kong, R., Gordon, E. M., Laumann, T. O., Zuo, X. N., Holmes, A. J., ... & Yeo, B. T. (2018). Local-global parcellation of the human cerebral cortex from intrinsic functional connectivity MRI. Cerebral cortex, 28(9), 3095-3114.

12. Tustison, N. J., Cook, P. A., Klein, A., Song, G., Das, S. R., Duda, J. T., ... & Avants, B. B. (2014). Large-scale evaluation of ANTs and FreeSurfer cortical thickness measurements. Neuroimage, 99, 166-179.

13. Wang, H., Suh, J. W., Das, S. R., Pluta, J. B., Craige, C., & Yushkevich, P. A. (2012). Multi-atlas segmentation with joint label fusion. IEEE transactions on pattern analysis and machine intelligence, 35(3), 611-623.

14. Yeh, F. C., & Tseng, W. Y. I. (2011). NTU-90: a high angular resolution brain atlas constructed by q-space diffeomorphic reconstruction. *Neuroimage*, *58*(1), 91-99.

15. Yeh, F. C., Badre, D., & Verstynen, T. (2016). Connectometry: a statistical approach harnessing the analytical potential of the local connectome. *Neuroimage*, *125*, 162-171
16. Yeo, B. T., Krienen, F. M., Sepulcre, J., Sabuncu, M. R., Lashkari, D., Hollinshead, M., ... & Buckner, R. L. (2011). The organization of the human cerebral cortex estimated by intrinsic functional connectivity. Journal of neurophysiology, 106(3), 1125-1165.

17. Yushkevich, P. A., Piven, J., Hazlett, H. C., Smith, R. G., Ho, S., Gee, J. C., & Gerig, G. (2006). User-guided 3D active contour segmentation of anatomical structures: significantly improved efficiency and reliability. *Neuroimage*, *31*(3), 1116-1128.

18. Yushkevich, P. A., Pluta, J. B., Wang, H., Xie, L., Ding, S. L., Gertje, E. C., ... & Wolk, D. A. (2015). Automated volumetry and regional thickness analysis of hippocampal subfields and medial temporal cortical structures in mild cognitive impairment. *Human brain mapping*, *36*(1), 258-287.

Acknowledgements

We would like to thank Mario Mendoza for his phlebotomy and MRI assistance at the UCSB Brain Imaging Center. We would like to thank Craig Stark and Rongwen Tain for MRI assistance at the UCI Facility for Imaging and Brain Research (FIBRE), and UCI Institute for Clinical and Translational Science for phlebotomy assistance. We would like to thank Bailey Tranquada-Torres, Rob Woodry, and Nikki Hatamian, for their assistance with data collection. Lastly, we would like to thank Magdalena Martínez-García, Susana Carmona, Scott Grafton, Javier Gonzalez-Castillo and Peter Bandettini for their insightful discussions and feedback on this project.

Funding

This study was supported by the Ann S. Bowers Women's Brain Health Initiative (EGJ, CT), UC Irvine Campus Funds (ERC), UC Academic Senate (EGJ), ReproGrants (HG, EGJ, ERC), NIH F99AG07979 (LP) and NIH AG063843 (EGJ). Authors J.F. and D.A.H. were supported by the Intramural Research Program of the National Institute of Mental Health (annual report ZIAMH002783).

Data Availability Statement

The dataset consists of 26 MRI scans (T1w, T2w, and diffusion scans) alongside state-dependent measures and serum assessments of ovarian sex hormones for each session. The data will be publicly available on https://openneuro.org/ upon publication. No custom code was used.